Paper Reprint:
Gruber Th., Rummel R., Concept and Capability of GOCE

MINISTERE DE LA CULTURE, DE L'ENSEIGNEMENT
SUPERIEUR ET DE LA RECHERCHE

Cahiers du Centre Européen de Géodynamique et de Séismologie

Volume 25

Proceedings of the Workshop:

GOCINA: Improving modelling of ocean transport and climate prediction in the North Atlantic region using GOCE gravimetry

April 13-15, 2005
Novotel, Luxembourg (Grand Duchy of Luxemburg)

Edited by
P. Knudsen, J. Johannessen, T. Gruber, S. Stammer and T. van Dam

Luxembourg 2006

Proceedings of the Workshop:

GOCINA: Improving modelling of ocean transport and climate prediction in the North Atlantic region using GOCE gravimetry

April 13-15, 2005

Novotel
Luxembourg-Kirchberg
Grand-Duchy of Luxembourg

Organized by
The European Center for Geodynamics and Seismology (ECGS)

Supported by

European Center for Geodynamics and Seismology (ECGS)
Ministère de la Culture, de l'Enseignement Supérieur et de la Recherche
Fonds National de la Recherche de Luxembourg
Musée national d'histoire naturelle
Danish National Space Center

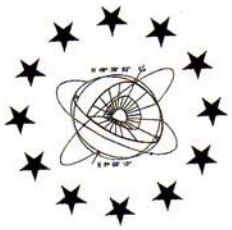

Scientific Organizing Committee:

P. Knudsen (DNSC, Denmark)
J. Johannessen (NERSC, Norway)
T. Gruber (IAPG, Germany)
D. Stammer (IfM, Germany)
T. van Dam (ECGS, Luxembourg)

Local Organizing Committee:

O. Francis (UL / ECGS, Luxembourg)
T. van Dam (ECGS, Luxembourg)
P. Codran (ECGS, Luxembourg)

Edited by:

P. Knudsen, J. Johannessen, T. Gruber, S. Stammer and T. van Dam
Luxembourg - 2006

PUBLIE AVEC LE SUPPORT DU

**MINISTERE DE LA CULTURE,
DE L'ENSEIGNEMENT SUPERIEUR ET DE LA RECHERCHE
&
FONDS NATIONAL DE LA RECHERCHE**

ISBN N° 2-9599804-2-5

Centre Européen de Géodynamique et de Séismologie

Musée national d'histoire naturelle
Section Astrophysique et Géophysique, Luxembourg

Imprimerie Centrale, 15 rue du Commerce, L- 1351 Luxembourg
Imprimé en 400 exemplaires

Concept and Capability of GOCE

Th. Gruber, R. Rummel
Institut für Astronomische und Physikalische Geodäsie (IAPG)
Technische Universität München, Arcistrasse 21, 80333 München, German
e-mail: Thomas.Gruber@bv.tu-muenchen.de

Abstract. In autumn 2006 the GOCE gradiometry ESA satellite mission will be launched. Its objective is the determination of a global model with maximum spatial resolution of the quasi-stationary gravity field and geoid. This makes the mission complementary to GRACE, which is designed so as to determine temporal variations of the Earth's gravity field with highest precision at long wavelengths. The gravity and geoid as derived from GOCE will be used in solid Earth geophysics, oceanography, geodesy and sea level research.

GOCE will be the first satellite to carry a gravity gradiometer and it will be for the first time that a sensor combination of gradiometer, GPS receiver and active angular and linear control systems will be flown in space. Consequently, a new data processing scheme has to be developed and adopted to this mission. It is the purpose of the GOCE ground segment elements to develop, test and operate the full processing chain for this new space-borne gravity sensor system in order to provide the projected precise GOCE gravity field model to the user community. The paper gives an overview of the GOCE mission concept, science goals and instruments as well as some details about the gradiometer data processing .

Keywords: Earth Observation, GOCE, Global Gravity Field Determination

1 Introduction

GOCE is the acronym for „Gravity field and steady-state Ocean Circulation Explorer mission". It is the first core satellite mission of the newly defined ESA "Living Planet" programme. The objective of GOCE is the determination of the stationary part of the Earth gravity field and geoid with highest possible spatial detail and precision. The gravity and geoid model derived from the GOCE mission will serve science and application in the fields of solid Earth physics, oceanography, geodesy and glaciology, compare (Johannessen et al, 2003; Rummel et al, 2002).

Two main applications can be distinguished. Firstly, the spatial variations of gravity and geoid are directly related to density anomalies in lithosphere and upper mantle, respectively, and consequently to interior stresses and ultimately to mass motion. In this respect GOCE provides important new information to studies of continental and oceanic lithosphere and upper mantle. Its information is complementary to that of seismic tomography, magnetic field models, geokinematic studies and laboratory results. Secondly, a detailed geoid surface when combined with satellite altimetry yields ocean topography, the quasi-stationary deviation of the actual mean ocean surface from its hypothetical surface of rest. Under the assumption of geostrophic balance ocean surface topography can be directly translated into a global map of ocean circulation. Thus, ocean surface circulation becomes directly measurable, globally and uninterruptedly. In conjunction with higher resolution ocean models and ocean measurements, GOCE is expected to improve significantly estimates of global mass and heat transport in the oceans (see Le Grand, 2003) . Furthermore, the global geoid will permit height systems to be connected globally with almost cm-precision. Sea level variations in Australia, or East Asia will become directly comparable to those measured in Europe or America. These and other expected scientific benefits from GOCE gravity and geoid models demonstrate that this mission represents an important element of global observation of mass anomalies, mass transport and mass exchange. The science goals and the requirements on the mission performance are summarized in Table 1.

To reach the science goals as specified above, precondition is that GOCE can determine gravity and geoid with a precision of 10^{-6}·g (corresponding to 1 mgal) and 1-2 cm, respectively, with a spatial resolution of better of 100 km half wavelength and that these results are achieved free of long wavelength systematic errors. The mission performance depends on the gravity sensor system on-board GOCE.

2 GOCE Mission Concept

Gravity measurements with CHAMP and GRACE are based on inter-satellite tracking. The concept of the GOCE satellite mission is the direct measurement of the anomalous static gravity field by pairs of accelerometers forming a 3-D gravity gradiometer. By observing differential accelerations in three directions in a drag-free environment (see chapter 3) and at very low altitude it will become possible to determine the gravity field globally to a much higher spatial resolution than with any satellite mission flown before. The gravity gradiometer, due to its short baseline between the accelerometers and due to

Application	Accuracy		Spatial Resolution (half wavelength – D in km)
	Geoid [cm]	Gravity [mgal]	
SOLID EARTH			
Lithosphere and upper mantle density structure		1-2	100
Continental lithosphere:			
▪ Sedimentary basins		1-2	50-100
▪ Rifts		1-2	20-100
▪ Tectonic motions		1-2	100-500
Seismic hazards		1	100
Ocean lithosphere and interaction with asthenosphere		0,5-1	100-200
OCEANOGRAPHY			
▪ Short scale	1-2		100
	0.2		200
▪ Basin scale	≈0.1		1000
ICE SHEETS			
▪ Rock basement		1-5	50-100
▪ Ice vertical movements	2		100-1000
GEODESY			
▪ Levelling by GPS	1		100-1000
▪ Unification of worldwide height systems	1		100-20000
▪ Inertial navigation system		≈1-5	100-1000
▪ Orbits		≈1-3	100-1000
SEA LEVEL CHANGE	Many of the above applications, with their specific requirements, are relevenat to studies of sea-level change.		

Table 1: Science Goals of the GOCE Mission (ESA, 1999)

its band limitation will not be able to observe the long wavelength part of the Earth gravity field with sufficient accuracy. Therefore it is complemented by high-low satellite-to-satellite tracking. A GPS-receiver will provide continuous position observations relative to the satellites of the GPS system. This part is identical to that of CHAMP, but due to the lower altitude of GOCE and due to the drag-free environment of the spacecraft some improvements in accuracy and resolution are expected. Figure 1 shows the general mission concept; Figure 2 provides an overview of the predicted performance of the GOCE mission compared to the predictions for CHAMP and GRACE and the results of some recent gravity field solutions from these two missions.

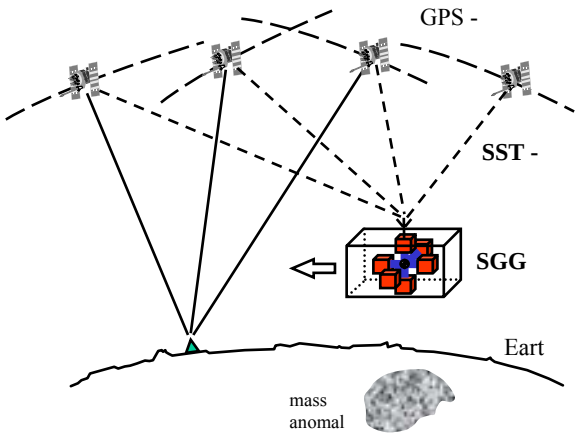

Figure 1: GOCE mission scenario with gravity gradiometry and high-low satellite-to-satellite tracking to the GPS constellation.

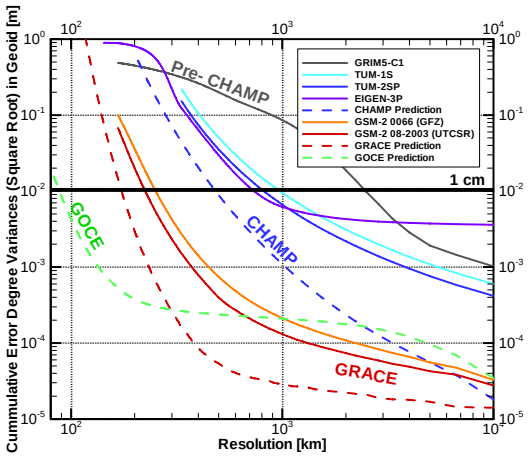

Figure 2: Square root of cummulative error degree variances from CHAMP, GRACE and GOCE mission prediction and from error estimates for some recent CHAMP models (blue) (TUM-1S, TUM-2SP, EIGEN-3P) and GRACE (red) (GFZ 66 days, CSR August 2003 monthly) gravity field models.

3 Instruments

Core instrument on-board GOCE is a three axis gravity gradiometer. It consists of three orthogonally mounted pairs of 3-axis accelerometers, i.e. an orthogonal arrangement of three one-axis gradiometers. The gradiometer baseline of each pair is about 50 cm long. The planned accelerometer precision is $10^{-12}\,\frac{m}{s^2}/\sqrt{Hz}$ along two axes with the third axis less sensitive. From the measured gravitational acceleration differences the three main diagonal terms of the gravitational tensor can be determined with high precision. The extremely high gradiometric

performance of the instrument is confined to the so-called measurement bandwidth (MBW). In addition, the gradiometer yields the required information of the angular acceleration about the out-of-plane axis (pitch) of the gradiometer. This information in combination with the angular rates as derived from the star sensor readings and from magnetometers is used as control signal for angular control of the spacecraft by magneto torquers. The use of magneto torquers implies that three-axis active angular control is possible only over part of each orbit revolution. In order to prevent non-gravitational forces acting on the spacecraft to "sneak" into the measured differential accelerations as secondary effect, the satellite is kept "drag-free" in along track direction by means of a pair of ion thrusters. The necessary control signal is derived from the available "common-mode" accelerations (=mean accelerations) along the three orthogonal axes of the accelerometer pairs of the gradiometer. The gradiometric and angular signal part of the common mode acceleration, which is a result of the imperfect symmetry of the gradiometer relative to the spacecraft centre of mass has to be modelled during data analysis.

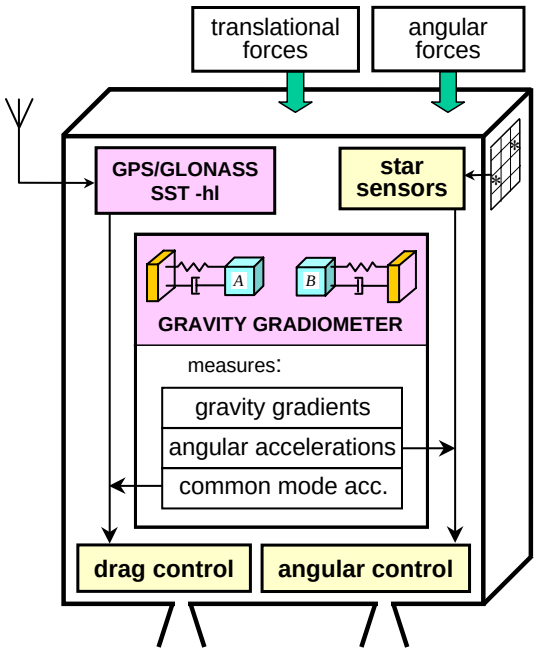

Figure 3: GOCE sensor concept for drag control, angular control and gravity gradiometry.

The second gravity sensor device is a newly developed GPS receiver. From its measurements the orbit trajectory is computed to within a few centimetres, either purely geometrically by a so-called kinematic orbit determination, or by the method of reduced dynamic orbit determination. As the spacecraft is kept in an almost drag-free mode (at least along track and within an extended measurement bandwidth) the orbit motion is purely gravitational. The observations from the GPS receiver complement the measurements of the gravity gradiometer. They provide high quality information about the long wavelength gravity field, below and at the lower end of the measurement bandwidth of the gradiometer. By a joint analysis of data from both gravity field sensors the final GOCE gravity field models are determined.

In summary, GOCE is a technologically very complex and demanding mission. The gravitational field sensor system consists of a three-axis gravitational gradiometer and a GPS receiver as core instruments. Orientation in inertial space is derived from star sensors, angular rates are deduced from the gradiometer. Common mode accelerations from the gradiometer are used for drag-free control with ion thrusters, magneto-torquers provide angular control. The principle of the system is shown in Figure 3 and, the system elements are summarized in Table 2.

Sensor	Measurements
3-axis gravity gradiometer	Gravity gradients Γ_{xx}, Γ_{yy}, Γ_{zz} in instrument system and in MBW (measurement bandwidth) Angular accelerations (high accurate around y-axis, less accurate around x, z axes) Common mode accelerations
Star sensors	High rate and high precision inertial orientation
GPS receiver	Orbit trajectory with cm-precision
Drag control with ion thruster	Control signal from common mode accelerations of gradiometer
Angular control with magnetic torquers	Based on angular rates from star sensors, magnetometer and gradiometer
Gradiometer calibration and quadratic factors	With cold gas thrusters (random pulses) and sinusoidal motion of test masses of accelerometers, respectively

Table 2: Summary of GOCE instruments.

4 Gradiometry with GOCE

As outlined in the previous chapter each accelerometer has two highly sensitive axes and one less sensitive axis. The directions of the less sensitive axes are identified in Figure 4 by the dashed arrows. They are orthogonal to the planes, which are defined by the two high sensitive axes of the accelerometers. The orientation in space of the six accelerometers forming the gravity gradiometer is as follows. Each pair of accelerometers along a baseline forms a one-axis gradiometer. These are the accelerometer pairs 1 and 4 (blue), 2 and 5 (yellow) and 3 and 6 (red) (see Figure 4). Nominally the one-axis gradiometers are orthogonal to each other with a common origin, which is close to the centre of mass of the satellite. The three vectors represented by the three one-axis gradiometer baselines form the so-called gradiometer reference frame (GRF). This is the frame where all observations of the gradiometer are taken. In addition, each accelerometer has its own reference frame (accelerometer reference frame), which is

aligned with the one-axis gradiometer baseline. The remaining two axes are parallel to the other two one-axis gradiometer baselines. Each triad forms a right-handed system in the origin of the accelerometer. Directions of the axes are shown in Figure 4. In space, nominally the three axes of the GRF are oriented such, that the x-axis points towards the flight direction, the y-axis is orthogonal to the orbital plane and the z-axis forms a right-handed system and points approximately away from the centre of the Earth. Due to the angular control by magneto-torquers, which enables active angular motion only towards the poles the GRF does not fully correspond to the nominal orientation in space as described above. During each half revolution small rotations about the x-axis and the z-axis with respect to the nominal orientation are present (by about ±3°).

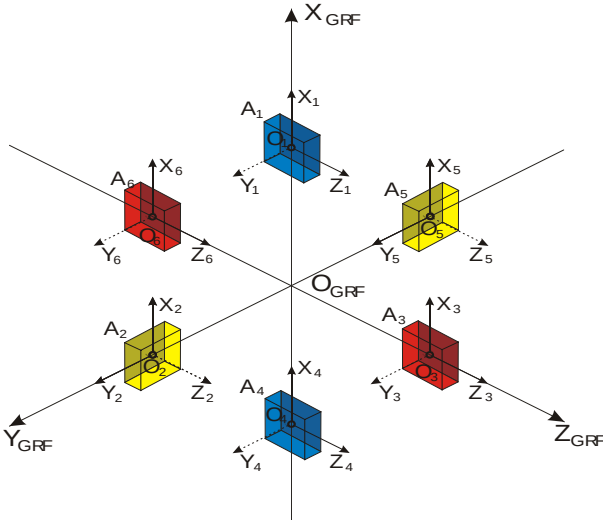

Figure 4: Schematic view of the three one-axis gradiometers, the gradiometer reference frame and the six accelerometer reference frames.

In the following the basic gradiometer equations are presented and it is shown, which parameters are determined from the highly sensitive axes and where there is an impact of the less sensitive axes (see also Rummel, 1986). All observations are taken in the GRF. The basic observation by one accelerometer under the assumption that accelerometer bias and scale factors, misalignments, centre of mass displacements, etc. are not present is defined by:

$$\underline{a} = -\underline{V}\cdot\underline{r} + \dot{\underline{\omega}}\times\underline{r} + \underline{\omega}\times(\underline{\omega}\times\underline{r}) \qquad (1)$$

with:

- $\underline{a}$ acceleration vector on proof mass
- $\underline{V}$ gravity gradient matrix
- $\underline{r}$ displacement of the accelerometer origin from the center of mass vector
- $\underline{\omega}$ angular rate vector
- $\dot{\underline{\omega}}$ angular acceleration vector

The three terms on the right hand side of equation (1) are caused by the following forces:

- 1st term: linear acceleration of accelerometer proof mass induced by the gravity field,
- 2nd term: linear acceleration of accelerometer proof mass induced by satellite angular accelerations
- 3rd term: centrifugal acceleration of accelerometer proof mass induced by satellite angular rotation

If we write equation (1) in the full form we get with (2), (3) and (4) the observation equation (5):

$$\underline{V}=\begin{pmatrix} V_{xx} & V_{xy} & V_{xz} \\ V_{yx} & V_{yy} & V_{yz} \\ V_{zx} & V_{zy} & V_{zz} \end{pmatrix};\ \underline{r}=\begin{pmatrix} r_x \\ r_y \\ r_z \end{pmatrix};\ \dot{\underline{\omega}}=\begin{pmatrix} \dot{\omega}_x \\ \dot{\omega}_y \\ \dot{\omega}_z \end{pmatrix};\ \underline{\omega}=\begin{pmatrix} \omega_x \\ \omega_y \\ \omega_z \end{pmatrix} \qquad (2)$$

$$\dot{\underline{\omega}}\times\underline{r}=\begin{pmatrix} \dot{\omega}_y r_z - \dot{\omega}_z r_y \\ \dot{\omega}_z r_x - \dot{\omega}_x r_z \\ \dot{\omega}_x r_y - \dot{\omega}_y r_x \end{pmatrix}=\begin{pmatrix} 0 & -\dot{\omega}_z & \dot{\omega}_y \\ \dot{\omega}_z & 0 & -\dot{\omega}_x \\ -\dot{\omega}_y & \dot{\omega}_x & 0 \end{pmatrix}\cdot\begin{pmatrix} r_x \\ r_y \\ r_z \end{pmatrix} \qquad (3)$$

$$\underline{\omega}\times(\underline{\omega}\times\underline{r})=\begin{pmatrix} \omega_x \\ \omega_y \\ \omega_z \end{pmatrix}\times\left\{\begin{pmatrix} \omega_x \\ \omega_y \\ \omega_z \end{pmatrix}\times\begin{pmatrix} r_x \\ r_y \\ r_z \end{pmatrix}\right\}=\begin{pmatrix} \omega_x \\ \omega_y \\ \omega_z \end{pmatrix}\times\begin{pmatrix} \omega_y r_z - \omega_z r_y \\ \omega_z r_x - \omega_x r_z \\ \omega_x r_y - \omega_y r_x \end{pmatrix}=$$
$$=\begin{pmatrix} \omega_x\omega_y r_y - \omega_y^2 r_x - \omega_z^2 r_x + \omega_x\omega_z r_z \\ \omega_y\omega_z r_z - \omega_z^2 r_y - \omega_x^2 r_y + \omega_x\omega_y r_x \\ \omega_x\omega_z r_x - \omega_x^2 r_z - \omega_y^2 r_z + \omega_y\omega_z r_y \end{pmatrix}=$$
$$=\begin{pmatrix} -\omega_y^2-\omega_z^2 & \omega_x\omega_y & \omega_x\omega_z \\ \omega_x\omega_y & -\omega_x^2-\omega_z^2 & \omega_y\omega_z \\ \omega_x\omega_z & \omega_y\omega_z & -\omega_x^2-\omega_y^2 \end{pmatrix}\cdot\begin{pmatrix} r_x \\ r_y \\ r_z \end{pmatrix} \qquad (4)$$

$$\begin{pmatrix} a_x \\ a_y \\ a_z \end{pmatrix}=\left\{-\begin{pmatrix} V_{xx} & V_{xy} & V_{xz} \\ V_{yx} & V_{yy} & V_{yz} \\ V_{zx} & V_{zy} & V_{zz} \end{pmatrix}+\begin{pmatrix} 0 & -\dot{\omega}_z & \dot{\omega}_y \\ \dot{\omega}_z & 0 & -\dot{\omega}_x \\ -\dot{\omega}_y & \dot{\omega}_x & 0 \end{pmatrix}+\begin{pmatrix} -\omega_y^2-\omega_z^2 & \omega_x\omega_y & \omega_x\omega_z \\ \omega_x\omega_y & -\omega_x^2-\omega_z^2 & \omega_y\omega_z \\ \omega_x\omega_z & \omega_y\omega_z & -\omega_x^2-\omega_y^2 \end{pmatrix}\right\}\begin{pmatrix} r_x \\ r_y \\ r_z \end{pmatrix} \qquad (5)$$

Now for each accelerometer $A_{1\text{-}6}$ the displacement vector relative to the centre of the GRF (assuming it is identical to the centre of mass) is introduced using the baseline length $L_{x,y,z}$ for each one-axis gradiometer.

$$A_1:\begin{pmatrix} r_x \\ r_y \\ r_z \end{pmatrix}=\begin{pmatrix} \frac{L_x}{2} \\ 0 \\ 0 \end{pmatrix};\ A_4:\begin{pmatrix} r_x \\ r_y \\ r_z \end{pmatrix}=\begin{pmatrix} -\frac{L_x}{2} \\ 0 \\ 0 \end{pmatrix} \qquad (6)$$

$$A_2:\begin{pmatrix} r_x \\ r_y \\ r_z \end{pmatrix}=\begin{pmatrix} 0 \\ \frac{L_y}{2} \\ 0 \end{pmatrix};\ A_5:\begin{pmatrix} r_x \\ r_y \\ r_z \end{pmatrix}=\begin{pmatrix} 0 \\ -\frac{L_y}{2} \\ 0 \end{pmatrix}$$

$$A_3:\begin{pmatrix} r_x \\ r_y \\ r_z \end{pmatrix}=\begin{pmatrix} 0 \\ 0 \\ \frac{L_z}{2} \end{pmatrix};\ A_6:\begin{pmatrix} r_x \\ r_y \\ r_z \end{pmatrix}=\begin{pmatrix} 0 \\ 0 \\ -\frac{L_z}{2} \end{pmatrix}$$

From equation (5) by introducing (6) the observation equations for each accelerometer (number index) in each axis (x,y,z index) can be written by (the green colour denotes observation along a high sensitive axis, red denotes observation along a less sensitive axis of the accelerometer):

$$
\begin{aligned}
a_{1,x} &= \left(-V_{xx} - \omega_y^2 - \omega_z^2\right)\frac{L_x}{2}; a_{4,x} = -\left(-V_{xx} - \omega_y^2 - \omega_z^2\right)\frac{L_x}{2} \\
a_{1,y} &= \left(-V_{yx} + \dot{\omega}_z + \omega_x \omega_y\right)\frac{L_x}{2}; a_{4,y} = -\left(-V_{yx} + \dot{\omega}_z + \omega_x \omega_y\right)\frac{L_x}{2} \\
a_{1,z} &= \left(-V_{zx} - \dot{\omega}_y + \omega_x \omega_z\right)\frac{L_x}{2}; a_{4,z} = -\left(-V_{zx} - \dot{\omega}_y + \omega_x \omega_z\right)\frac{L_x}{2}
\end{aligned} \tag{7}
$$

$$
\begin{aligned}
a_{2,x} &= \left(-V_{xy} - \dot{\omega}_z + \omega_x \omega_y\right)\frac{L_y}{2}; a_{5,x} = -\left(-V_{xy} - \dot{\omega}_z + \omega_x \omega_y\right)\frac{L_y}{2} \\
a_{2,y} &= \left(-V_{yy} - \omega_x^2 - \omega_z^2\right)\frac{L_y}{2}; a_{5,y} = -\left(-V_{yy} - \omega_x^2 - \omega_z^2\right)\frac{L_y}{2} \\
a_{2,z} &= \left(-V_{zy} + \dot{\omega}_x + \omega_y \omega_z\right)\frac{L_y}{2}; a_{5,z} = -\left(-V_{zy} + \dot{\omega}_x + \omega_y \omega_z\right)\frac{L_y}{2}
\end{aligned} \tag{8}
$$

$$
\begin{aligned}
a_{3,x} &= \left(-V_{xz} + \dot{\omega}_y + \omega_x \omega_z\right)\frac{L_z}{2}; a_{6,x} = -\left(-V_{xz} + \dot{\omega}_y + \omega_x \omega_z\right)\frac{L_z}{2} \\
a_{3,y} &= \left(-V_{yz} - \dot{\omega}_x + \omega_y \omega_z\right)\frac{L_z}{2}; a_{6,y} = -\left(-V_{yz} - \dot{\omega}_x + \omega_y \omega_z\right)\frac{L_z}{2} \\
a_{3,z} &= \left(-V_{zz} - \omega_x^2 - \omega_y^2\right)\frac{L_z}{2}; a_{6,z} = -\left(-V_{zz} - \omega_x^2 - \omega_y^2\right)\frac{L_z}{2}
\end{aligned} \tag{9}
$$

These are the basic equations for all further deviations. They are treated here as idealized, free of any systematic errors like misalignments, scale factors, biases etc.

Common-Mode Accelerations

Common-mode (or mean) accelerations are computed from the mean of two accelerometers of one one-axis gradiometer in each direction.

$$a_{c,l,k,i} = \frac{1}{2}\left(a_{l,i} + a_{k,i}\right) \tag{10}$$

with: c = common mode
l = 1st accelerometer number
k = 2nd accelerometer number
I = direction (x,y,z)

By introducing equations (7) for the one axis accelerometer pair 1 and 4 it becomes obvious that all common-mode accelerations cancel to zero in the nominal case. The same is true for the accelerometer pairs 2, 5 and 3, 6, respectively. In other words, this means that in an optimal case the drag-free control system works perfectly and the control loop automatically sets all resulting common-mode accelerations to zero. The perfect scenario means that the common-mode accelerations determined by the on-board Software are perfectly translated to ion-propulsion and they perfectly eliminate the impact of the non-conservative forces acting on the satellite. In reality it can not be expected that the observed common-mode accelerations will always become zero. The remaining signal can be addressed to imperfections of the drag-free control system, to imperfections of the in-orbit calibration of the gradiometer and to misalignments of the gradiometer axes or centre of mass displacement. In order to optimally exploit the gradiometer observations these remaining common-mode accelerations have to be carefully analyzed and taken into consideration during observation pre-processing as residual accelerations from non-conservative forces. What also becomes visible from equations (7) to (9) is, that the common-mode accelerations in flight direction (x-axis) are observed by all three accelerometer pairs with the highly sensitive axes. This means that in the direction of the main signal of non-conservative forces some internal control is possible. In contrast, the common-mode accelerations in cross-track (y-axis) and radial direction (z-axis) are observed only by one or two highly sensitive accelerometer axes, respectively.

Differential-Mode Accelerations

Differential-mode accelerations are computed by subtracting the observations of the two accelerometers of each one one-axis gradiometer in each direction.

$$a_{d,l,k,i} = \frac{1}{2}\left(a_{l,i} - a_{k,i}\right) \tag{11}$$

with: d = differential model
l = 1st accelerometer number
k = 2nd accelerometer number
I = direction (x,y,z)

By introducing equation (7) the differential-mode accelerations e.g. for the accelerometer pair 1 and 4 are computed by the following formulas (the meaning of the colours is identical as described before).

$$
\begin{aligned}
a_{d,l,4,x} &= \frac{1}{2}\left(a_{1,x} - a_{4,x}\right) = \\
&= \frac{1}{2}\left(-V_{xx} - \omega_y^2 - \omega_z^2\right)\frac{L_x}{2} + \frac{1}{2}\left(-V_{xx} - \omega_y^2 - \omega_z^2\right)\frac{L_x}{2} = \\
&= \frac{L_x}{4}\left(-2V_{xx} - 2\omega_y^2 - 2\omega_z^2\right) = \frac{L_x}{2}\left(-V_{xx} - \omega_y^2 - \omega_z^2\right)
\end{aligned} \tag{12}
$$

$$a_{d,1,4,y} = \frac{1}{2}\left(a_{1,y} - a_{4,y}\right) = \\ = \frac{1}{2}\left(-V_{yx} + \dot{\omega}_z + \omega_x\omega_y\right)\frac{L_x}{2} + \frac{1}{2}\left(-V_{yx} + \dot{\omega}_z + \omega_x\omega_y\right)\frac{L_x}{2} = \\ = \frac{L_x}{4}\left(-2V_{yx} + 2\dot{\omega}_z + 2\omega_x\omega_y\right) = \frac{L_x}{2}\left(-V_{yx} + \dot{\omega}_z + \omega_x\omega_y\right) \quad (13)$$

$$a_{d,1,4,z} = \frac{1}{2}\left(a_{1,z} - a_{4,z}\right) = \\ = \frac{1}{2}\left(-V_{zx} - \dot{\omega}_y + \omega_x\omega_z\right)\frac{L_x}{2} + \frac{1}{2}\left(-V_{zx} - \dot{\omega}_y + \omega_x\omega_z\right)\frac{L_x}{2} = \\ = \frac{L_x}{4}\left(-2V_{zx} - 2\dot{\omega}_y + 2\omega_x\omega_z\right) = \frac{L_x}{2}\left(-V_{zx} - \dot{\omega}_y + \omega_x\omega_z\right) \quad (14)$$

Analogously the differential mode accelerations for the accelerometer pairs 2, 5 and 3, 6 become:

$$a_{d,2,5,x} = \frac{1}{2}\left(a_{2,x} - a_{5,x}\right) = \frac{L_y}{2}\left(-V_{xy} - \dot{\omega}_z + \omega_x\omega_y\right) \quad (15)$$

$$a_{d,2,5,y} = \frac{1}{2}\left(a_{2,y} - a_{5,y}\right) = \frac{L_y}{2}\left(-V_{yy} - \omega_x^2 - \omega_z^2\right) \quad (16)$$

$$a_{d,2,5,z} = \frac{1}{2}\left(a_{2,z} - a_{5,z}\right) = \frac{L_y}{2}\left(-V_{zy} + \dot{\omega}_x + \omega_y\omega_z\right) \quad (17)$$

$$a_{d,3,6,x} = \frac{1}{2}\left(a_{3,x} - a_{6,x}\right) = \frac{L_z}{2}\left(-V_{xz} + \dot{\omega}_y + \omega_x\omega_z\right) \quad (18)$$

$$a_{d,3,6,y} = \frac{1}{2}\left(a_{3,y} - a_{6,y}\right) = \frac{L_z}{2}\left(-V_{yz} - \dot{\omega}_x + \omega_y\omega_z\right) \quad (19)$$

$$a_{d,3,6,z} = \frac{1}{2}\left(a_{3,z} - a_{6,z}\right) = \frac{L_z}{2}\left(-V_{zz} - \omega_x^2 - \omega_y^2\right) \quad (20)$$

Equations (12) to (20) provide the basic quantities for computation of the gravity gradients, which are the fundamental observables of the gravity field. The angular accelerations $\dot{\omega}$, which are required together with the star camera measurements for angular control of the satellite also are computed from the differential model accelerations.

The nine differential accelerations divided by the corresponding baseline lengths constitute the basic 3x3 matrix of gradiometric observations. It is composed of these symmetric matrices, the gravity gradient and the centrifugal component matrix and of the skew-symmetric matrix of angular accelerations. This property, symmetry versus anti-symmetry, allows the separation of the angular acceleration components from the gradiometric and centrifugal ones, in principle.

Gradiometer Angular Rates

The angular accelerations of the spacecraft with respect to the three axes of the GRF are derived from linear combinations of the differential mode accelerations. From these angular accelerations angular rates are computed by integration over time. These angular rates are determined purely from the accelerometer readings, while the angular rates finally used for the angular control and the data processing are determined by a spectral combination of these accelerometer derived angular rates with those derived by differentiation from the star tracker observations. Both sensor systems provide complementary information (long frequency information from the star trackers, high frequency angular rates from the accelerometers). The following equations shall identify which angular acceleration (and after integration which angular rate) is determined from highly sensitive accelerometer axes and where the less sensitive axes influence the derived angular rates.

From equations (17) and (19) we get:

$$\dot{\omega}_x = \frac{2a_{d,2,5,z}}{L_y} + V_{zy} - \omega_y\omega_z \quad ; \quad \dot{\omega}_x = -\frac{2a_{d,3,6,y}}{L_z} - V_{yz} + \omega_y\omega_z \quad (21)$$

By addition of both equations (21) we get the observation equation for the angular accelerations about the x-axis (roll).

$$2\dot{\omega}_x = -\frac{2a_{d,3,6,y}}{L_z} - V_{yz} + \omega_y\omega_z + \frac{2a_{d,2,5,z}}{L_y} + V_{zy} - \omega_y\omega_z \quad (22)$$

$$\dot{\omega}_x = -\frac{a_{d,3,6,y}}{L_z} + \frac{a_{d,2,5,z}}{L_y}$$

In analogy the angular accelerations about the y-axis (pitch) and z-axis (yaw) are determined from equations (14) and (18) and equations (13) and (15) respectively.

$$\dot{\omega}_y = -\frac{a_{d,1,4,z}}{L_x} + \frac{a_{d,3,6,x}}{L_z} \quad (23)$$

$$\dot{\omega}_z = \frac{a_{d,1,4,y}}{L_x} - \frac{a_{d,2,5,x}}{L_y} \quad (24)$$

From equations (22) to (24) it can be seen that the angular control with respect to the y-axis, which represents the largest rotational component of the spacecraft, can be determined very accurately, while the determination of rotations about the x-axis and to some extent also about the z-axis is weak. The spacecraft will rotate about these two axes only by a few degrees with slowly varying angular rates. This means that the main signal of the angular rates will be in the lower frequency spectrum. As star trackers provide good information for low frequencies and accelerometers provide good information in the medium to high frequencies, it is obvious that the angular rates computation about the x- and z-axes relies heavily on the star tracker information.

Gravity Gradients

The gravity gradients, which represent the central observables for gravity field determination with GOCE are computed directly from or by linear combinations of the differential mode accelerations. The diagonal components of the gravity gradient tensor are computed from equations (12), (16) and (20) using:

$$V_{xx} = -\frac{2a_{d,1,4,x}}{L_x} - \omega_y^2 - \omega_z^2 \quad (25)$$

$$V_{yy} = -\frac{2a_{d,2,5,y}}{L_y} - \omega_x^2 - \omega_z^2 \quad (26)$$

$$V_{zz} = -\frac{2a_{d,3,6,z}}{L_z} - \omega_x^2 - \omega_y^2 \quad (27)$$

The off-diagonal elements of the gravity tensor are computed by linear combinations of equations (13) and (15), (14) and (18) and (17) and (19), respectively.

$$V_{xy} = -\frac{a_{d,1,4,y}}{L_x} - \frac{a_{d,2,5,x}}{L_y} + \omega_x\omega_y \quad (28)$$

$$V_{xz} = -\frac{a_{d,1,4,z}}{L_x} - \frac{a_{d,3,6,x}}{L_z} + \omega_x\omega_z \quad (29)$$

$$V_{zy} = -\frac{a_{d,2,5,z}}{L_y} - \frac{a_{d,3,6,y}}{L_z} + \omega_y\omega_z \quad (30)$$

Inspection of equations (25) to (30) shoes that the gravity gradients for the z-y component are solely determined from differential mode accelerations of less sensitive accelerometer axes. This implies that this gravity gradient tensor component does not provide sufficiently accurate information to be used for the gravity field processing. This is also true for the x-y gravity gradient component. Differential mode accelerations based on highly sensitive axes of the accelerometers are used to compute the remaining 4 components, which include all diagonal components. They contain the main signal of the gravity field to be determined. The quality of the gravity gradients is also influenced by the angular rates. As explained above, these rates are computed by integrating the accelerometer derived angular accelerations and by combining them with angular rates derived from the star tracker readings. From the equations above it becomes obvious that specifically the angular rates about the x- and z-axis have to be improved by the star tracker information in order to minimize the impact of less sensitive accelerometer axes on the diagonal terms of the gravity gradient tensor.

5 Conclusions

The GOCE satellite will be the first mission observing the gravity field directly from space with a gravity gradiometer. The gravity gradiometer is the core instrument. It is complemented by a GPS-receiver, star tracker, magnetometers, magnetic torquers fro angular control and ion-thrusters fro along-track drag control. All systems together constitute the GOCE gravity sensor system. For this reason it is required that all system elements are understood correctly and that their interactions are taken into account during ground processing. This is well reflected in the gradiometer equations as they are described in the paper. From their analysis the following conclusions can be drawn:

- Common mode accelerations in flight direction are determined solely from highly sensitive accelerometer observations. These common mode accelerations are used for the drag-free control system. As the main non-gravitational forces are acting in flight direction this represents the optimal strategy. The still remaining common mode accelerations are an important information source.
- The dominating angular motion is the rotation once per revolution about the y-axis. Because of the deviation of the GRF from the local orbit system and due to the attitude control concept based on magnetorquers, the angular rates about the x- and z-axes are slowly varying within each revolution. The angular rate reconstruction procedure determines an optimal estimate for all angular rates by combining the accelerometer derived angular rates with the star tracker derived angular rates. Actually the angular rates, which are partly or fully determined by the less sensitive accelerometer axes are strongly improved by the star tracker information.
- The diagonal gravity gradient tensor elements as well as the x-z tensor component are determined from highly sensitive differential accelerations. Angular rates to be applied for their computation are partly derived from the less sensitive axes. This means that the performance of the angular rate reconstruction algorithm has implication on the quality of the gravity gradients.

References

ESA: *Reports for Mission Selection 'The Four Candidate Earth Explorer Core Missions', Gravity Field and Steady-State Ocean Circulation Mission*; ESA SP-1233(1), ESA Publication Division, 1999.

Johanessen J., Balmino G., LeProvost C., Rummel R., Sabadini R., Sünkel H., Tschenring C.C., Visser P., Woodworth P., Hughes C., LeGrand P., Sneeuw N., Perosanz F., Aguirre-Martinez M., Rebhan H., Drinkwater M.: *The European Gravity Field and steady-state Ocean Circulation Explorer satellite mission: Its impact on Geophysics*. Surveys in Geophysics, Kluwer Academic Publishers, 2003.

LeGrand P.: *Impact of Geoid Improvement on Ocean Mass and Heat Transport Estimates*; Space Science Reviews, Vol. 108, No. 1-2, pp. 225-238, 2003.

Rummel R.: *Satellite Gradiometry*; in: Lecture Notes in Earth Sciences, Vol. 7, pp. 317-363, Mathematical and Numerical Techniques in Physical Geodesy; Ed. H. Sünkel, Springer Berlin, 1986.